Magnetic flux avalanches in Nb/NbN thin films

L. B. L. G. Pinheiro*,† M. Caputo‡,§ C. Cirillo‡,§ C. Attanasio§,‡ T. H. Johansen,¶ W. A. Ortiz,† A. V. Silhanek,‖ and M. Motta†**

December 20, 2019

Abstract

Technological applications of NbN thin films may be threatened by the development of magnetic flux avalanches of thermomagnetic origin appearing in a large portion of the superconducting phase. In this work we describe an approach to substantially suppress the magnetic flux avalanche regime, without compromising the upper critical field. This procedure consists of depositing a thin Nb layer before the reactive deposition of NbN, thus forming a bi-layered system. We use AC susceptibility and DC magnetometry to characterize both the single layer films, Nb and NbN, and the bi-layered specimen, as well as calibrated Magneto-Optical Imaging to map the instability regime of the studied samples. Magnetic flux imaging reveals interesting features of the dendritic flux avalanches in the bi-layer system, including halo-like patterns and crossing avalanches.

keywords: Bi-layer, proximity effect, anti-avalanches, halo-like structure, crossing avalanches.

*Instituto Federal de São Paulo, Campus São Carlos, 13565-905 São Carlos, SP, Brazil.

†Departamento de Física, Universidade Federal de São Carlos, 13565-905 São Carlos, SP, Brazil.

‡CNR-SPIN, c/o Università degli Studi di Salerno, I-84084 Fisciano (Sa), Italy.

§Dipartimento di Fisica "E. R. Caianiello", Università degli Studi di Salerno, FI-84084 Fisciano (Sa), Italy.

¶Department of Physics, University of Oslo, POB 1048, Blindern, 0316 Oslo, Norway.

‖Experimental Physics of Nanostructured Materials, Q-MAT, CESAM, Université de Liège, B-4000 Sart Tilman, Liège, Belgium.

**corresponding author: m.motta@df.ufscar.br

1 Introduction

According to the Bardeen-Stephen model [1], moving flux quanta dissipate energy due to the existence of an electric field through the normal core of each flux tube. The electric field accelerates the quasiparticles at the core thereby increasing their energy. This energy raising process is normally compensated by the energy relaxation rate of quasiparticles by means of their inelastic scattering [2]. Larkin and Ovchinnikov [3] realized that at high vortex velocities and correspondingly to high electric fields, the energy of quasiparticles can reach the superconducting gap, and diffuse into the superconducting phase surrounding the vortex core. As a consequence, the quasiparticle density in the vortex core is reduced and the vortex shrinks. The higher the vortex speed, the larger the deficit of quasiparticles at the core, the smaller its size and therefore the lower the damping coefficient η. If η decreases with increasing v, an instability point in the viscous flux flow is reached when the damping force $\eta(v)v$ starts to decline as v increases. A single vortex moving at such high velocities will then leave a wake of quasiparticles behind its path which can be regarded as a trail of depleated order parameter. Naturally, other moving vortices will find energetically favorable to follow the same path, and therefore a rearrangement of the Abrikosov vortex lattice is expected [4]. Eventually, these rivers of rapidly moving vortices, directly observed in Ref. [5, 6], can transform into a phase slip line [7]. Note that the mechanism described above involves a non-thermal change of the distribution function of quasiparticles trapped in the vortex cores. Bezuglyj and co-authors [8, 9] theoretically demonstrated that for magnetic fields above a certain threshold, the Larkin-Ovchinnikov instability switches to a pure thermal instability of flux flow resulting from the heating of quasiparticles.

The scenario described above corresponds to a bulk three-dimensional superconductor. When treating thin film geometries, where the penetration depth λ is larger than the thichness d of the film, an additional complication arises due to the fact that magnetic flux diffusion becomes strongly nonlocal and the vortex interaction is, to a large extent, mediated by the magnetic stray field and the screening of the in-plane supercurrents [10]. In this case, fastly moving flux quanta triggered either by a bias current [11, 12] or by magnetic field changes [13] will then act as precursors of thermomagnetic flux avalanches [14].

These events consist of abrupt bursts of magnetic flux rushing into the sample, usually taking the form of dendrite-like structures. Their branches avoid each other during their growth [15], as reported both in experiments and in simulations using the thermomagnetic (TM) model [16, 17]. This model describes the TM instabilities as the source of the flux avalanches, and predicts the existence of a threshold flux penetration depth (l^*) needed to trigger them. Once the penetration depth reaches l^*, the first burst takes place and the instability regime lasts until l^* is equal to half of the sample size [18, 19, 20]. Therefore, an upper and lower threshold fields [20] can be identified as the borders of the instability region for a isothermal field ramping. By means of magnetization measurements, Colauto *et al.* [21] were able to delineate a region on the magnetic field-temperature diagram where instabilities occur in a 200 nm thick Nb film. Among other materials, dendritic flux avalanches were also observed in NbN films, spanning over a large window of fields and temperatures [22].

Niobium nitride has higher critical field ($H_{C2}(T)$) and critical temperature (T_C) than pure Nb [23], what makes it NbN more suitable for superconducting devices [24], such as hot-electron bolometers [25], high-frequency superconducting circuits [26, 27], single-photon detectors [28], and qubits for quantum computers [29], to name a few. Some applications may suffer from unwanted TM instabilities. Yurchenko *et al.* [30] have shown that such abrupt phenomena can be prevented by covering the NbN film with a copper coating. Independently, the idea of depositing a superconducting coating to enhance the applicability range was investigated in references [31, 32, 33]. In these works it was shown that the stability improvement in superconducting wires covered by a thin superconductor depends on the electrical and thermal properties of both. Such a system becomes more stable if the capping layer has lower critical current density and higher heat capacity. Moreover, Ivry and co-workers [34] have proposed to use a thin proximitized bi-layer structure NbN/WSi to optimize the performance of superconducting single photon detectors.

Stacks of overlapping but electrically disconnected superconducting thin films is another way to affect the avalanche regimes, as demonstrated by Tamegai *et al.* [35]. They studied the critical states and thermomagnetic avalanche activities in three-dimensional nanostructured superconductors, i.e., stacks of Nb strips, insulated from each other by SiO_2 layers. Here, it was shown that flux avalanches can start in one layer and end at another. Although the avalanche activity has been shown to be reduced in superconducting films capped with a normal metal [30, 36], thermomagnetic instabilities were not reported so far in bi-layered systems where NbN is in intimate contact with other superconducting layer. In this context, we present in this paper an approach capable of enhancing the potential applicability of NbN thin films by systematically exploring the avalanche regime in a bi-layer system composed of Nb and NbN thin films.

2 Experimental Details

In order to perform a comparative analysis of the magnetic flux avalanche regime, 15 nm thick Nb (Nb15) and 60 nm thick NbN (NbN60) single films and hybrids (NbN/Nb) were deposited on Si(100) substrates at room temperature in a UHV DC diode magnetron sputtering system with a base pressure in the low of 10^{-8} mbar range. The Ar pressure, during the deposition of the Nb layer, was $P_{Ar} = 2.5 \cdot 10^{-3}$ mbar, while NbN was reactively sputtered in an atmosphere of Ar and N_2, with $P_{Ar} = 2.5 \cdot 10^{-3}$ mbar and $P_{N_2} = 0.7 \cdot 10^{-3}$ mbar. The deposition rates were $r_{Nb} = 0.26$ nm/s for Nb and $r_{NbN} = 0.17$ nm/s for NbN, as measured by a quartz crystal monitor previously calibrated by measuring the step height of photolithographically patterned films with a Bruker DektakXT stylus profiler. Samples with different structures were deposited by keeping the thickness of the Nb and NbN individual layers constant, namely $d_{Nb} = 15$ nm and $d_{NbN} = 60$ nm.

All the studied samples, having approximately the same area of 4×4 mm^2, were characterized by AC susceptometry and DC magnetometry in a commercial MPMS 5 Quantum Design magnetometer. Magneto-Optical Imaging (MOI) experiments, based on the Faraday effect [37], was carried out by placing a $Bi_xY_{1-x}FeO$ indicator [38] on top of the superconducting film. More details about the MOI setup can be found elsewhere [39, 40]. In all measurements, the field H was applied perpendicular to the film surface. We also perfomed a numerical convertion from pixel intensity of magneto-optical (MO) images to the local magnetic flux density (B), mapping B_z all over the sample and its neighborhood, following the protocol reported in Ref. [41].

3 Results and Discussion

3.1 Upper critical field

The critical temperature of superconducting thin films is thickness dependent and usually lower than the bulk values [42]. The onset critical temperature (T_C) of the samples were determined by AC susceptibility measurements, presented in Figure 1(a), showing the following values: (6.90 ± 0.05) K for Nb15; (10.50 ± 0.05) K for the NbN60, and (10.00 ± 0.05) K for the hybrid sample. The critical temperature for the NbN film is close to values reported in the literature for similar thicknesses [43, 44]. It is also important to mention that T_C of the single NbN layer is 0.5 K above of that the bi-layer, which is assumed here to be a consequence of growing the NbN film on top of the Nb layer already deposited on the substrate.

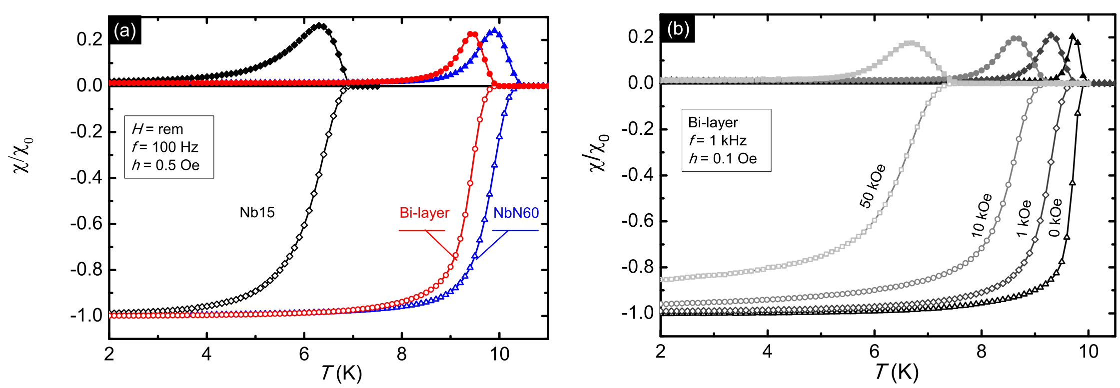

Figure 1: AC susceptibility *vs* temperature for all the investigated films (a) and for different applied magnetic fields H for the bi-layer system (b). The y axis is normalized by χ_0, which is the Meissner plateau value for the in-phase component of the AC susceptibility for each sample. The frequency (f) and the amplitude (h) of the AC excitation are indicated in each panel.

The fact that we do not observe a double or a broader transition in the bi-layer with respect to the single layer films is a relevant hint suggesting highly transparent proximity effect [45] in between the layers. The absence of a double transition in the bi-layer sample remains for applied magnetic fields up to $H = 50$ kOe, as shown in Figure 1(b). The existence of the proximity effect in the bi-layer specimen was also confirmed by a double transition in a sample with an additional 5 nm thick Nb_2O_5 insulating layer between the superconducting films (data not shown here).

By performing susceptibility measurements as a function of temperature for H up to 50 kOe, we determined the H_{C2} vs t diagram presented in Figure 2, t being the reduced temperature, $t = \frac{T}{T_c}$. We estimate the $H_{C2}(0)$ values by fitting to the data the expression $H_{C2}(t) = H_{C2}(0) \cdot (1 - t^2)$, plotted as dashed lines in the same graph. For both the bi-layer and NbN60 films, $H_{C2}(0)$ is close to 110 kOe, whereas for the Nb15 film it is approximately 27 kOe. Based on the derivative of the upper critical field versus temperature near T_C, we determined the superconducting coherence lengths at 0 K ($\xi(0)$) of 10.7 nm, 4.7 nm, and 4.6 nm, for Nb15, NbN60, and the bi-layer, respectively. We did not detect flux avalanches in AC susceptibility measurements using driving fields up to 3.8 Oe, consistently with the existing literature [46, 47], since avalanches occur only at higher fields.

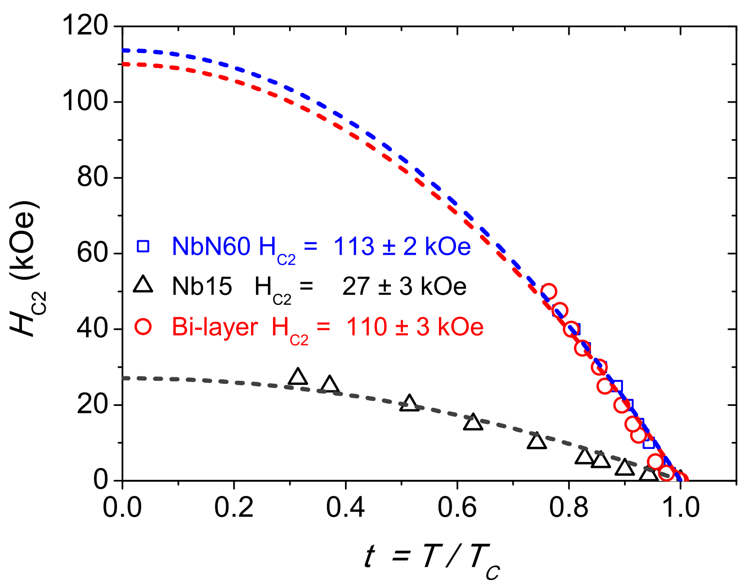

Figure 2: H_{C2} versus reduced temperature $t = T/T_c$ for Nb15, NbN60 and the bi-layer, showing the extrapolated upper critical field at $T = 0$ K.

3.2 Flux jumps regime

In order to identify the instability regimes of these systems, we measured the DC magnetization as a function of the applied magnetic field at the same reduced temperature $t = 0.3$. The result is presented in Figure 3. The presence of magnetic flux jumps is clearly identified, for all samples as a noisy magnetic response, being particularly prominent for the NbN sample. Note, however, that avalanche activity is strongly suppressed by the proximitized Nb layer (bi-layer sample).

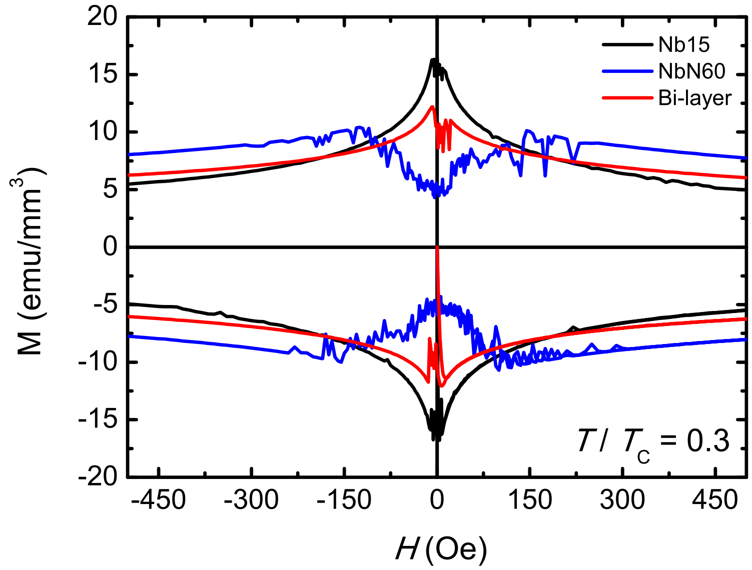

Figure 3: DC magnetization as a function of the applied magnetic field at $t = \frac{T}{T_C} = 0.3$. The noisy response at low fields observed in all samples corresponds to the presence of magnetic flux jumps.

The critical current density (J_C) is a crucial parameter determining whether the thermomagnetic avalanches will take place [48]. The higher the J_C the larger the probability of observing flux jumps. Based on the Bean critical state model [49], one can roughly estimate J_C by the difference between the increasing and decreasing branches of the magnetization loop. This approach is acceptable in the smooth part of the magnetization loop (i.e. without flux jumps). A direct inspection of Figure 3 shows that the critical current densities are rather similar for all samples, whereas the avalanche activity in the bi-layer sample has decreased as compared to that in the NbN single layer.

3.3 Magneto-Optical Imaging

Flux avalanches disrupting the smooth penetration after a zero field cooling (ZFC) procedure can be visualized in the MO images of Figure 4(a), for each of the investigated films. In all those MO images, the brighter the pixel, the higher perpendicular flux density. While large dendritic flux avalanches are observed in both NbN60 and Nb15 films, the bi-layer system exhibits much less activity, only some small finger-like avalanches occurring from the left and right edges. By changing the temperature, magnetization loops allow one to delineate the instability region in the applied magnetic field versus reduced temperature (H-t) diagram shown in Figure 4(b). This figure presents one of the main messages from this work, namely a substantial enlargement of the stability regime, i.e. where only smooth flux penetration occurs, of the bi-layer system as compared to the bare NbN film. In other words, the bi-layer instability regime (in green) shrinks toward that of the Nb15 one (in yellow).

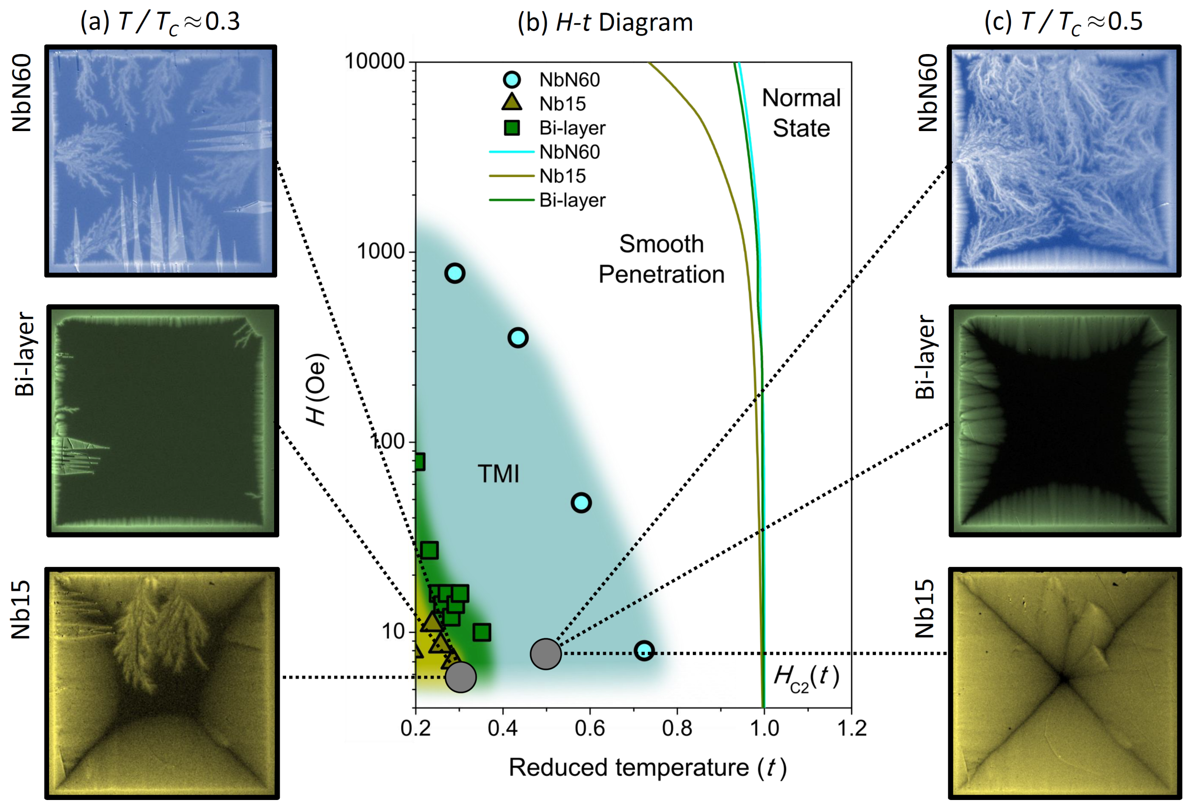

Figure 4: Column (a) shows MO images for each studied samples at $t \approx 0.3$ and $H = 4$ Oe. The zig-zag-like features in the images are related to domain walls in the indicator film. (b) H-t diagram showing the thermomagnetic instabilities regime (TMI) as a function of the reduced temperature; (c) MO images taken at $t \approx 0.5$ and $H = 8.5$ Oe.

When $t \approx 0.5$, the NbN60 sample exhibits avalanches, as presented in the top MO image in Figure 4 (c). Both the bi-layer and the Nb15 films show smooth penetration, with the latter one in the fully flux penetrated state. All the flux avalanches presented in Figure 4 show positive flux only, i.e., they were created following the virgin curve of the magnetization loop by increasing the applied field from zero. By decreasing the applied magnetic field in a superconducting film, after keeping flux trapped into the sample, negative field-polarity avalanches, or simply anti-avalanches, can occur. Anti-avalanches can show an annihilation zone [15, 50], i.e., a boundary of zero flux density separating the regions of flux and antiflux, which coexists due to the application of moderate reverse fields in a sample with flux already trapped by the pinning centers. This terminology has been used to describe the contour of anti-avalanches in the early stage of MO investigations of the abrupt flux penetration in superconducting thin films [15].

Once anti-avalanches are created by decreasing the applied magnetic field, their onset depends on the previous magnetic history of the system. Figure 5(a)-(e) presents quantitative MO images obtained at certain magnetic fields along the hysteresis loop of the NbN/Nb bilayer sample at $T = 3.5$ K. The spatial profile of the induction component $B_z(r)$ at the bottom of each image has been obtained from an average of 40 lines as shown by the translucent yellow bar in panel (a).

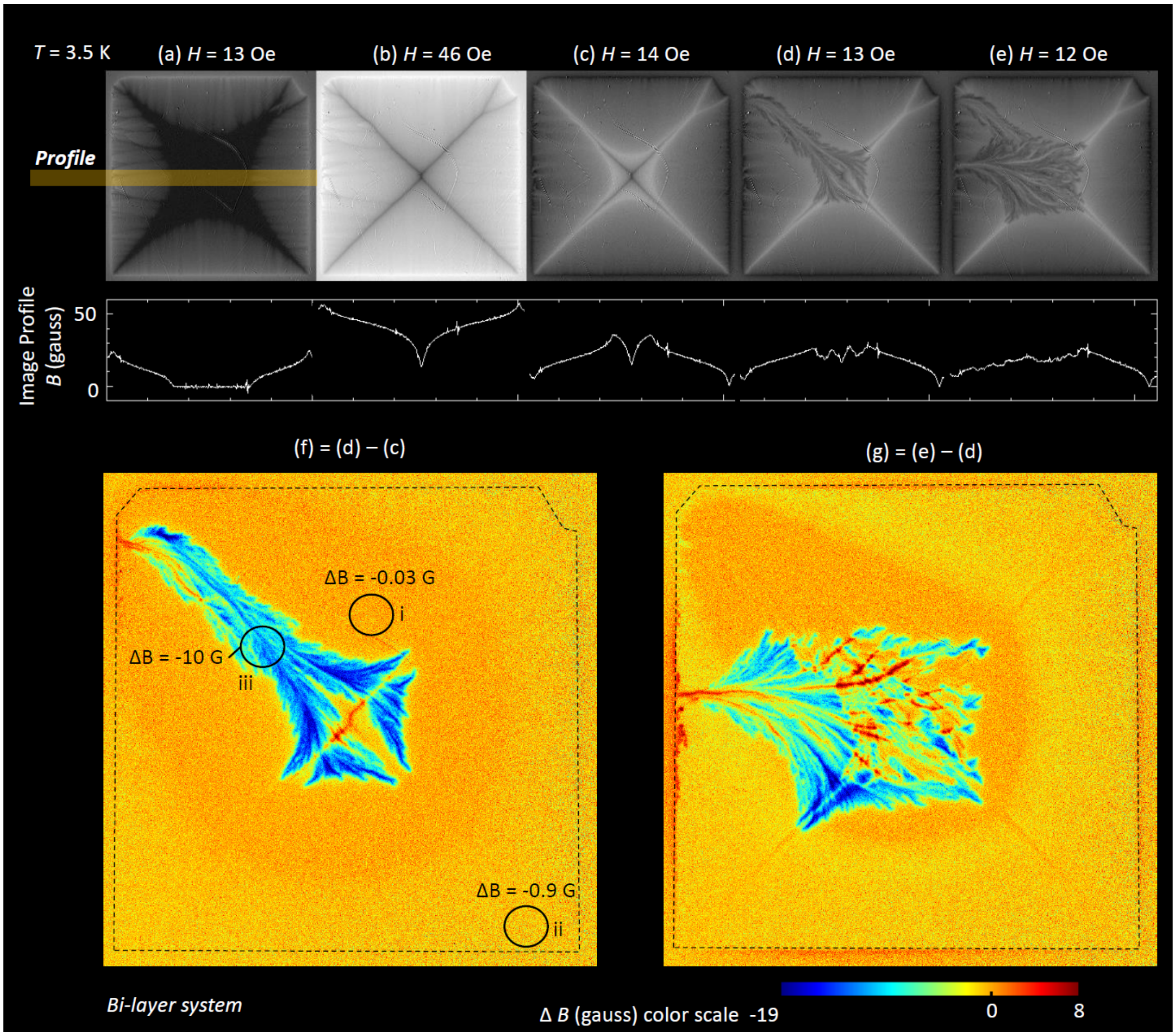

Figure 5: (a)-(e) A sequence of quantitative MO images of the bi-layer system, for different applied magnetic fields, after a ZFC procedure, at $T = 3.5\ K$. At the bottom of each panel the field profile is shown, averaged from 40 lines delimited by the translucid yellow bar identified in panel (a). (f) Differential image obtained by subtracting (d) and (c) panels, which shows the first anti-avalanche and an orange halo surrounding it. The field variation ΔB is indicated by black circles, (i) inside the halo, (ii) outside the halo, and (iii) inside the avalanche. (g) Differential image between panels (e) and (d), where the second anti-avalanche crosses the first one. The color scale indicates that the trapped field increased in some regions where the avalanche branches cross. The dashed lines in panels (f) and (g) are indications of the sample edges.

Figure 5(a) shows a typical critical state-like field profile for the virgin curve in a magnetization loop where the inner part of the film is still in the Meissner state (dark inner area), i.e., $B = 0$. In panel (b), the applied field reaches its maximum value ($H = 46$ Oe), and $B > 0$ at the center of the sample. The diagonal dark lines forming an X shape pattern are named discontinuity lines (d-lines), and delineate the locations where the supercurrent undergoes an abrup change of direction. Panel (c) shows the flux density landscape after decreasing H down to 14 Oe starting from its maximum value, and just before the occurrence of the first anti-avalanche in the system. The field profile in panel (c) reveals a large quantity of positive flux trapped in the sample. The first anti-avalanche (d) starts from the top left corner into the positive upper left d-line. This preferential track suggests that most likely this avalanche is driven by the flux-antiflux annihilation process. The magnetic profile at the bottom of panel (d) shows the recorded imprint of this anti-avalanche, and it does not change the polarity of the induction field B along its path, but strongly decreases the local field as it passes. By decreasing the applied magnetic field by 1 Oe, another anti-avalanche is triggered from the left edge, transpassing the center of the sample and then crossing the first avalanche of anti-flux. The second anti-avalanche does not change the local field to negative values, although it decreases further the average B in the whole sample. Nevertheless, these two anti-avalanches exhibit particular features that can be better emphasized by implementing differential MOI [51], i.e. by subtracting consecutively recorded images. The result of this procedure is presented in panels (f) and (g) of Figure 5.

Note that the first anti-avalanche running along the d-line produces end branches directed along the crossing d-line. A remarkable feature is the appearance of a halo surrounding the anti-avalanche, a feature that, to the best of our knowledge, has not been reported so far. To describe this halo in a quantitative form, we measured the average variation of B in three circular regions with 25,000 pixels each in different regions throughout the sample. The result is marked by the black circles seen in panel (f). The circle (i), inside the halo itself, is the region where the local field decreased less ($\Delta B_i = -0.03$ G). This procedure was done in other points across the halo (not shown), to confirm this observation. Outside the halo, the circle (ii) results in $\Delta B_{ii} = -0.9$ G, and inside the avalanche (circle (iii)), the average flux density variation from this area was $\Delta B_{iii} = 16\text{ G} - 26\text{ G} = -10$ G. According to the color scale, one can see that there are regions in the anti-avalanche branches where the field variation is as high as -19 G. The differential MO image in panel (f) allows one to state that the average field in the sample decreased. The trapped flux in the system seems to lead to this unexpected halo. More details on the halo structure and its surroundings are provided in the supplementary material. The sample Nb15 also shows a halo-like structure around its first anti-avalanche, but this halo was not detected in the film NbN60. The halo is not a thick annihilation zone, as one can see in the B profile of Figure 5 (d) and (e) $-$ there is no crossover between positive to negative flux there, and thus, no zero-field region. This halo refers to the absence of rearrangement of the flux distribution in the region around the abrupt penetration during the first anti-avalanche.

Another intriguing aspect of this set of images is that the second anti-avalanche crosses the first one. The color scale in Figure 5(g) allows one to highlight the fact that the branches of the first avalanche transpassed by the second one, undergo a positive variation of the local magnetic field as high as 8 G. Flux avalanches triggered during a ZFC procedure are known for avoiding each other during their propagation into the sample [15], no matter whether they are small and fingerlike or large and highly branched. However, avalanches may cross each other in descending fields because there is still positive flux where the prior anti-avalanche passed. Although the halo of the first anti-avalanche has changed after the advent of the second avalanche, this last one does not have a halo surrounding it.

3.4 Halo definition

What we call halo is a region of extra brightness (in our case, ΔB) surrounding the first anti-avalanche for the bi-layer system. Figure 6 (a) is a differential image, as presented in Figure 5 (f). Panels (b), (c) and (d) are the averaged ΔB profiles for three regions of the sample, indicated by translucent gray bars. Panel (b) shows the ΔB profile passing through the avalanche trunk, where there is an intense negative variation of B ($\Delta B < 0$), as well as a smooth variation close to the sample edges (outside the halo). In (c), the halo region presents the highest brightness in the whole image ($\Delta B = 0$). Panel (d) present a region outside the halo where ΔB is negative and constant. Therefore, the halo is suitable to describe such a region in the framework of differential images.

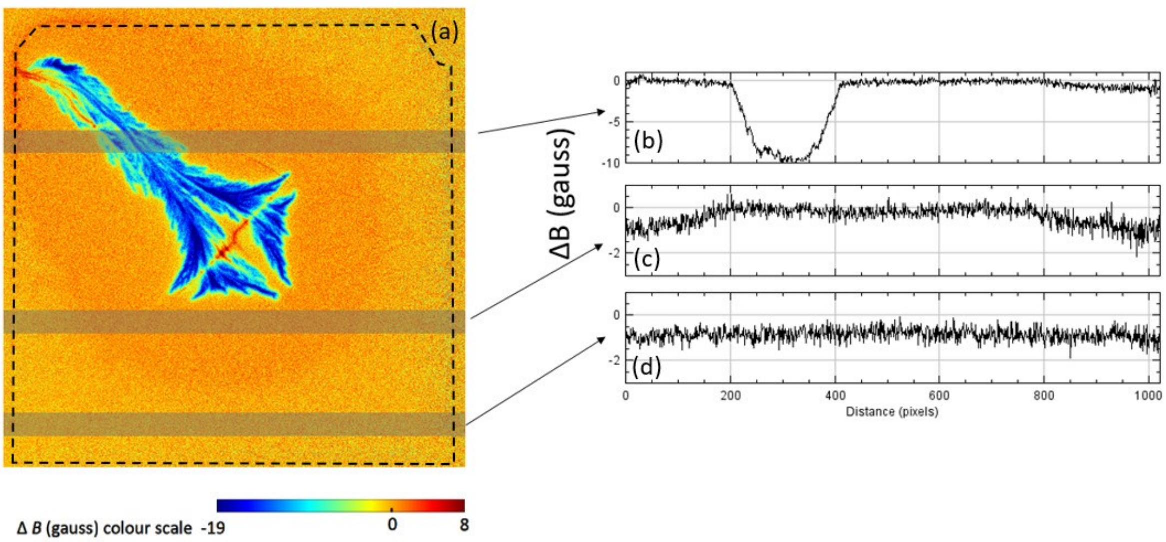

Figure 6: Description of the halo structure. (a) Differential image obtained by subtracting (d) and (c) panels of Figure 5, presented as panel (f). Averaged ΔB profiles taken from the translucent gray bars, passing through (b) the anti-avalanche, (c) the halo, and (d) outside the halo.

4 Conclusions

In this paper we propose an approch to reduce the flux avalanche activity in NbN films by coating them with a Nb layer. This measure may improve the applicability of thin films of NbN without changing its upper critical field at the same reduced temperature. A similar effect has been reported when the superconductive film is coated with a normal metal [30, 36, 52, 53, 54, 55]. The region where the avalanches take place in the field-reduced temperature diagram decreases for the hybrid system as compared to the single NbN layer, becoming closer to the single Nb film. In other words, there is a suppression of the occurrence of flux avalanches in the hybrid NbN/Nb system without considerably depreciating its other properties. In addition to that, quantitative MOI allows one to unveil anti-avalanches crossing, as well as the lack of vortex rearrangement in a large region surrounding the first anti-avalanche. This latter effect manifests itself as a halo of nearly unperturbed magnetic field intensity.

5 Acknowledgements

This work was partially supported by the National Council for Scientific and Technological Development (CNPq), by the Coordenação de Aperfeiçoamento de Pessoal de Nível Superior - Brasil (CAPES) - Finance Code 001, by the Brazilian program Science without Borders, and by the Norwegian Research Council. The authors thank the COST action NanoCoHybri (CA16218). AVS acknowledge support from the Fonds de la Recherche Scientifique – FNRS.

References

[1] J. Bardeen and M. J. Stephen. Theory of the motion of vortices in superconductors. *Phys. Rev.*, 140:A1197–A1207, Nov 1965.

[2] W. Klein, R. P. Huebener, S. Gauss, and J. Parisi. Nonlinearity in the flux-flow behavior of thin-film superconductors. *Journal of Low Temperature Physics*, 61(5-6):413–432, December 1985.

[3] A. I. Larkin and Yu. N. Ovchinnikov. Nonlinear conductivity of superconductors in the mixed state. *Soo. Phys. JETP*, 41(5):960–965, 1976.

[4] D. Y. Vodolazov and F. M. Peeters. Rearrangement of the vortex lattice due to instabilities of vortex flow. *Phys. Rev. B*, 76:014521, Jul 2007.

[5] A. V. Silhanek, M. V. Milošević, R. B. G. Kramer, G. R. Berdiyorov, J. Van de Vondel, R. F. Luccas, T. Puig, F. M. Peeters, and V. V. Moshchalkov. Formation of stripelike flux patterns obtained by freezing kinematic vortices in a superconducting Pb film. *Phys. Rev. Lett.*, 104:017001, Jan 2010.

[6] L. Embon, Y. Anahory, Ž.L. Jelić, E. O. Lachman, Y. Myasoedov, M. E. Huber, G. P. Mikitik, A. V. Silhanek, M. V. Milošević, A. Gurevich, and E. Zeldov. Imaging of super-fast dynamics and flow instabilities of superconducting vortices. *Nature Communications*, 8(1), July 2017.

[7] A. Andronov, I. Gordion, V. Kurin, I. Nefedov, and I. Shereshevsky. Kinematic vortices and phase slip lines in the dynamics of the resistive state of narrow superconductive thin film channels. *Physica C: Superconductivity and its Applications*, 213(1):193 – 199, 1993.

[8] A. I. Bezuglyj and V. A. Shklovskij. Effect of self-heating on flux flow instability in a superconductor near T_c. *Physica C: Superconductivity*, 202(3):234 – 242, 1992.

[9] A. I. Bezuglyj, V. A. Shklovskij, R. V. Vovk, V. M. Bevz, M. Huth, and O. V. Dobrovolskiy. Local flux-flow instability in superconducting films near T_c. *Phys. Rev. B*, 99:174518, May 2019.

[10] E. H. Brandt. The flux-line lattice in superconductors. *Reports on Progress in Physics*, 58(11):1465–1594, nov 1995.

[11] A. V. Bobyl, D. V. Shantsev, T. H. Johansen, W. N. Kang, H. J. Kim, E. M. Choi, and S. I. Lee. Current-induced dendritic magnetic instability in superconducting MgB_2 films. *Applied Physics Letters*, 80(24):4588–4590, 2002.

[12] D. Carmo, F. Colauto, A. M. H. de Andrade, A. A. M. Oliveira, W. A. Ortiz, and T. H. Johansen. Controllable injector for local flux entry into superconducting films. *Superconductor Science and Technology*, 29(9):095003, july 2016.

[13] E. Altshuler and T. H. Johansen. Colloquium: Experiments in vortex avalanches. *Rev. Mod. Phys.*, 76:471–487, Apr 2004.

[14] I. S. Aranson, A. Gurevich, M. S. Welling, R. J. Wijngaarden, V. K. Vlasko-Vlasov, V. M. Vinokur, and U. Welp. Dendritic flux avalanches and nonlocal electrodynamics in thin superconducting films. *Phys. Rev. Lett.*, 94:037002, Jan 2005.

[15] T. H. Johansen, M. Baziljevich, D. V. Shantsev, P. E. Goa, Y. M. Galperin, W. N. Kang, H. J. Kim, E. M. Choi, M.-S. Kim, and S. I. Lee. Dendritic flux patterns in MgB_2 films. *Superconductor Science and Technology*, 14:726–728, 2001.

[16] I. Aranson, A. Gurevich, and V. Vinokur. Vortex avalanches and magnetic flux fragmentation in superconductors. *Phys. Rev. Lett.*, 87:067003, Jul 2001.

[17] D. V. Denisov, A. L. Rakhmanov, D. V. Shantsev, Y. M. Galperin, and T. H. Johansen. Dendritic and uniform flux jumps in superconducting films. *Phys. Rev. B*, 73:014512, Jan 2006.

[18] D. V. Denisov, D. V. Shantsev, Y. M. Galperin, E. M. Choi, H. S. Lee, S. I. Lee, A. V. Bobyl, P. E. Goa, A. A. F. Olsen, and T. H. Johansen. Onset of dendritic flux avalanches in superconducting films. *Phys. Rev. Lett.*, 97:077002, Aug 2006.

[19] E. M. Choi, H. S. Lee, J. Y. Lee, S. I. Lee, Å. A. F. Olsen, V. V. Yurchenko, D. V. Shantsev, T. H. Johansen, H. J. Kim, and M. H. Cho. Width-dependent upper threshold field for flux noise in MgB_2 strips. *Applied Physics Letters*, 91(4):042507, 2007.

[20] V. V. Yurchenko, D. V. Shantsev, T. H. Johansen, M. R. Nevala, I. J. Maasilta, K. Senapati, and R. C. Budhani. Reentrant stability of superconducting films and the vanishing of dendritic flux instability. *Phys. Rev. B*, 76:092504, Sep 2007.

[21] F. Colauto, E. J. Patiño, M. G. Blamire, and W. A. Ortiz. Boundaries of the instability region on the HT diagram of Nb thin films. *Superconductor Science and Technology*, 21(4):045018, mar 2008.

[22] I. A. Rudnev, D. V. Shantsev, T. H. Johansen, and A. E. Primenko. Avalanche-driven fractal flux distributions in NbN superconducting films. *Applied Physics Letters*, 87(4):1–4, 2005.

[23] M. Ashkin, J. R. Gavaler, J. Greggi, and M. Decroux. The upper critical field of NbN films. ii. *Journal of Applied Physics*, 55(4):1044–1048, 1984.

[24] D. Hazra, N. Tsavdaris, S. Jebari, A. Grimm, F. Blanchet, F. Mercier, E. Blanquet, C. Chapelier, and M. Hofheinz. Superconducting properties of very high quality NbN thin films grown by high temperature chemical vapor deposition. *Superconductor Science and Technology*, 29(10):105011, sep 2016.

[25] I. Tretyakov, S. Ryabchun, M. Finkel, A. Maslennikova, K. Natalia, A. Lobastova, B. Voronov, and G. Gol'tsman. Low noise and wide bandwidth of NbN hot-electron bolometer mixers. *Applied Physics Letters*, 98(3):033507, January 2011.

[26] V. Michal, S. Bouat, J. Villegier, and J. Sedlacek. Superconducting NbN band-pass filter and matching circuit for 30 GHz RSFQ data converter. In *2009 19th International Conference Radioelektronika*, pages 161–164, April 2009.

[27] V. Larrey, J. . Villegier, M. Salez, F. Miletto-Granozio, and A. Karpov. Processing and characterization of high J_c NbN superconducting tunnel junctions for THz analog circuits and RSFQ. *IEEE Transactions on Applied Superconductivity*, 9(2):3216–3219, June 1999.

[28] R. Cheng, C.-L. Zou, X. Guo, S. Wang, X. Han, and H. X. Tang. Broadband on-chip single-photon spectrometer. *Nature Communications*, 10(1), September 2019.

[29] W. Qiu, K. Makise, H. Terai, Y. Nakamura, and Z. Wang. Measurement of quality factor and losses in superconducting microwave resonator integrated with NbN/AlN/NbN qubit circuit. *Journal of Physics: Conference Series*, 507(PART 4), 2014.

[30] V. V. Yurchenko, A. J. Qviller, S. Chaudhuri, I. J. Maasilta, D. V. Shantsev, Y. M. Galperin, and T. H. Johansen. Suppression of magnetic flux avalanches and recovery of the critical state in superconducting NbN films, 2012.

[31] P. Fabbricatore, M. Greco, C. Ferdeghini, C. Bernini, U. Gambardella, G. Celentano, and A. Devred. Low-field instabilities in Nb_3Sn multifilamentary wires: The possible role of unreacted Nb. *Superconductor Science and Technology*, 20(6):2–5, 2007.

[32] S. V. Vasiliev, O. M. Chumak, V. V. Chabanenko, F. Pérez-Rodríguez, and A. Nabiałek. Stability of bilayer superconductors against thermomagnetic avalanche. *Acta Physica Polonica A*, 126(4A):A84–A87, 2014.

[33] O. M. Chumak, V. V. Chabanenko, V. F. Rusakov, S. V. Vasiliev, F. Pérez-Rodríguez, and A. Nabiałek. Threshold Field for Runaway Instability of Bilayer Hard Type-II Superconductor. *Journal of Low Temperature Physics*, 179(1-2):75–82, 2015.

[34] Y. Ivry, J. J. Surick, M. Barzilay, C.-S. Kim, F. Najafi, E. Kalfon-Cohen, A. D. Dane, and K. K. Berggren. Superconductor – superconductor bilayers for enhancing single-photon detection. *Nanotechnology*, 28:Art. n. 435205, 2017.

[35] T. Tamegai, A. Mine, Y. Tsuchiya, S. Miyano, S. Pyon, Y. Mawatari, and S. Nagasawa. Superconductivity and its applications Critical states and thermomagnetic instabilities in three-dimensional nanostructured superconductors. *Physica C: Superconductivity and its applications*, 533:74–79, 2017.

[36] J. Brisbois, V. N. Gladilin, J. Tempere, J. T. Devreese, V. V. Moshchalkov, F. Colauto, M. Motta, T. H. Johansen, J. Fritzsche, O.-A. Adami, N. D. Nguyen, W. A. Ortiz, R. B. G. Kramer, and A. V. Silhanek. Flux penetration in a superconducting film partially capped with a conducting layer. *Phys. Rev. B*, 95:094506, Mar 2017.

[37] Ch. Jooss, J. Albrecht, H. Kuhn, S. Leonhardt, and H. Kronmüller. Magneto-optical studies of current distributions in $high - T_c$ superconductors. *Reports on Progress in Physics*, 65(5):651–788, apr 2002.

[38] L. E. Helseth, R. W. Hansen, E. I. Il'yashenko, M. Baziljevich, and T. H. Johansen. Faraday rotation spectra of bismuth-substituted ferrite garnet films with in-plane magnetization. *Phys. Rev. B*, 64:174406, Oct 2001.

[39] F. Colauto, M. Motta, A. Palau, M. G. Blamire, T. H. Johansen, and W. A. Ortiz. First observation of flux avalanches in a-MoSi superconducting thin films. *IEEE Transactions on Applied Superconductivity*, 25(3), 2015.

[40] L. E. Helseth, A. G. Solovyev, R. W. Hansen, E. I. Il'yashenko, M. Baziljevich, and T. H. Johansen. Faraday rotation and sensitivity of (100) bismuth-substituted ferrite garnet films. *Phys. Rev. B*, 66:064405, Aug 2002.

[41] G. Shaw, J. Brisbois, L. B.G.L. Pinheiro, J. Müller, S. Blanco Alvarez, T. Devillers, N. M. Dempsey, J. E. Scheerder, J. Van De Vondel, S. Melinte, P. Vanderbemden, M. Motta, W. A. Ortiz, K. Hasselbach, R. B.G. Kramer, and A. V. Silhanek. Quantitative magneto-optical investigation of superconductor/ferromagnet hybrid structures. *Review of Scientific Instruments*, 89(2), 2018.

[42] M. Faucher, T. Fournier, B. Pannetier, C. Thirion, W. Wernsdorfer, J. C. Villegier, and V. Bouchiat. Niobium and niobium nitride SQUIDs based on anodized nanobridges

made with an atomic force microscope. *Physica C: Superconductivity*, 368(1):211 – 217, 2002.

[43] J. R. Gavaler, M. A. Janocko, A. Patterson, and C. K. Jones. Very High Critical Current and Field Characteristics of Niobium Nitride Thin Films. *Journal of Applied Physics*, 42(1):54–57, 1971.

[44] J. H. Tyan and J. T. Lue. Grain boundary scattering in the normal state resistivity of superconducting NbN thin films. *Journal of Applied Physics*, 75(1):325–331, 1994.

[45] I. Giaever and K. Megerle. Study of superconductors by electron tunneling. *Physical Review*, 122(4):1101–1111, 1961.

[46] A. V. Silhanek, S. Raedts, and V. V. Moshchalkov. Paramagnetic reentrance of ac screening: Evidence of vortex avalanches in Pb thin films. *Physical Review B - Condensed Matter and Materials Physics*, 70(14):5–7, 2004.

[47] M. Motta, F. Colauto, R. Zadorosny, T. H. Johansen, R. B. Dinner, M. G. Blamire, G. W. Ataklti, V. V. Moshchalkov, A. V. Silhanek, and W. A. Ortiz. Visualizing the ac magnetic susceptibility of superconducting films via magneto-optical imaging. *Physical Review B*, 84(21):214529, dec 2011.

[48] R. Mints and A. Rakhmanov. Critical state stability in type-II superconductors and superconducting-normal-metal composites. *Reviews of Modern Physics*, 53(3):551–592, July 1981.

[49] C. P. Bean. Magnetization of hard superconductors. *Phys. Rev. Lett.*, 8:250–253, Mar 1962.

[50] E. Baruch-El, M. Baziljevich, T. H. Johansen, and Y. Yeshurun. Substrate Influence on Dendritic Flux Instability in YBCO Thin Films. *Journal of Superconductivity and Novel Magnetism*, 28:379–382, 2015.

[51] A. Soibel, E. Zeldov, M. Rappaport, Y. Myasoedov, T. Tamegai, S. Ooi, M. Konczykowskl, and V. B. Geshkenbein. Imaging the vortex-lattice melting process in the presence of disorder. *Nature*, 406(6793):282–287, 2000.

[52] E. M. Choi, H. S. Lee, H. J. Kim, B. Kang, S. I. Lee, A. A. F. Olsen, D. V. Shantsev, and T. H. Johansen. Dendritic magnetic avalanches in carbon-free mgb_2 thin films with and without a deposited Au layer. *Applied Physics Letters*, 87(15):152501, October 2005. WOS:000232442200043.

[53] J. Albrecht, A. T. Matveev, M. Djupmyr, G. Schütz, B. Stuhlhofer, and H.-U. Habermeier. Bending of magnetic avalanches in mgb_2 thin films. *Applied Physics Letters*, 87(18):182501, 2005.

[54] P. Mikheenko, A. J. Qviller, J. I. Vestgården, S. Chaudhuri, I. J. Maasilta, Y. M. Galperin, and T. H. Johansen. Nanosecond voltage pulses from dendritic flux avalanches in superconducting NbN films. *Applied Physics Letters*, 102(2):022601, 2013.

[55] J. Brisbois, B. Vanderheyden, F. Colauto, M. Motta, W. A. Ortiz, J. Fritzsche, N. D. Nguyen, B. Hackens, O.-A. Adami, and A. V. Silhanek. Classical analogy for the deflection of flux avalanches by a metallic layer. *New Journal of Physics*, 16(10):103003, October 2014.